

# Short-timescale fluctuations in the difference light curves of QSO 0957+561A,B: microlensing or noise ?

R. Gil-Merino<sup>1,2</sup>, L.J. Goicoechea<sup>1</sup>, M. Serra-Ricart<sup>3</sup>, A. Oscoz<sup>3</sup>, D. Alcalde<sup>3</sup> and E. Mediavilla<sup>3</sup>

<sup>1</sup> *Departamento de Física Moderna, Universidad de Cantabria, Avda. Los Castros s/n, E-39005 Santander, Spain*

*E-mail: gilmerino@unican.es, goicol@unican.es*

<sup>2</sup> *Lehrstuhl Astrophysik, Institut für Physik, Universität Potsdam, Am Neuen Palais 10, D-14469 Potsdam, Germany*

*E-mail: rmerino@astro.physik.uni-potsdam.de*

<sup>3</sup> *Instituto de Astrofísica de Canarias, Via Láctea s/n, La Laguna, E-38200 Spain*

*E-mail: mserra@iac.es, aoscoz@iac.es, dalcalde@iac.es, emg@iac.es*

Accepted 2000 October 10

## ABSTRACT

From optical R band data of the double quasar QSO 0957+561A,B, we made two new difference light curves (about 330 days of overlap between the time-shifted light curve for the A image and the magnitude-shifted light curve for the B image). We observed noisy behaviours around the zero line and no short-timescale events (with a duration of months), where the term event refers to a prominent feature that may be due to microlensing or another source of variability. Only one event lasting two weeks and rising - 33 mmag was found. Measured constraints on the possible microlensing variability can be used to obtain information on the granularity of the dark matter in the main lensing galaxy and the size of the source. In addition, one can also test the ability of the observational noise to cause the rms averages and the local features of the difference signals. We focused on this last issue. The combined photometries were related to a process consisting of an intrinsic signal plus a Gaussian observational noise. The intrinsic signal has been assumed to be either a smooth function (polynomial) or a smooth function plus a stationary noise process or a correlated stationary process. Using these three pictures without microlensing, we derived some models totally consistent with the observations. We finally discussed the sensitivity of our telescope (at Teide Observatory) to several classes of microlensing variability.

**Key words:** gravitational lensing – dark matter – galaxies: elliptical and lenticular, cD – quasars: individual: Q0957+561

## 1 INTRODUCTION

### 1.1 Microlensing caused by the Galaxy and other spirals

Dark matter dominates the outer mass of the Milky Way. In principle, the population of the Galactic dark halo may include astrophysical objects as black holes, brown dwarfs, cool white dwarfs, etc., i.e., MACHOs (massive compact halo objects) with stellar or substellar mass, as well as elementary particles (a smooth component). Today, from microlensing surveys, we have some information about the granular component (MACHOs). The absence of very short duration events implies that the dark halo cannot be dominated by planetary objects. A joint analysis by *EROS* and *MACHO* collaborations indicated that MACHOs in the mass range  $10^{-7}M_{\odot} \leq M \leq 10^{-3}M_{\odot}$  make up less than 25% of the

dark halo (Alcock et al. 1998). From a likelihood analysis, the *MACHO* collaboration concluded that a population of objects of mass  $\sim 0.5 M_{\odot}$  is consistent with their first two year of data. These MACHOs with stellar mass would have an important contribution to the total mass (Alcock et al. 1997; Gould 1997; Sutherland 1999; Mao 2000). However, very recent results by the *MACHO* team, based on approximately six years of observations, point to a relatively small mass fraction (Alcock et al. 2000). For a typical size halo, the maximum likelihood estimates suggest the existence of a Milky Way dark halo consisting of about 20% MACHOs with mass of  $\sim 0.6 M_{\odot}$ . The *EROS* collaboration also agrees with this small contribution to the dark halo by  $\sim 0.6 M_{\odot}$  objects (Lasserre et al. 2000). Lasserre et al. (2000) derived strong upper limits on the abundance of MACHOs with different masses. For example, < 10% of the dark halo resides in planetary objects. Moreover, they ruled out a standard

spherical halo in which more than 40% of its mass is made of dark stars with  $1 M_{\odot}$ . Finally, we remark that the Milky Way dark halo inferred from the likelihood method (best standard fits by Alcock et al. 2000) is consistent with the *HST* (Hubble Space Telescope) detection of a halo white dwarf population (Ibata et al. 1999). A population of cool white dwarfs contributing 1/5 of the dark matter in the Milky Way could explain all new observational results, but the hypothesis presents some difficulties (e.g., Mao 2000; Alcock et al. 2000).

The information on the nature of galaxy dark haloes is still largely based on a local spiral galaxy (the Galaxy), and so, the study of other galaxies seems an interesting goal.

The Einstein Cross (QSO 2237+0305) is a  $z = 1.69$  quasar lensed by a face-on barred Sb galaxy at  $z = 0.0394$ . The time delay between the four quasar images is expected to be less than a day (Rix et al. 1992; Wambsganss & Paczyński 1994), and so, one can directly separate intrinsic variability from microlensing signal. For this lens system, light rays of the 4 images pass through the bulge of the foreground galaxy and there is a robust evidence that microlensing events occur (e.g., Irwin et al. 1989; Wozniak et al. 2000). The observed events may be interpreted as a phenomenon caused by the granularity of the matter associated with the nearby spiral. Very recently, for providing an interpretation of the *OGLE* Q2237+0305 microlensing light curve, Wyithe, Turner & Webster (2000) used the contouring technique of Lewis et al. (1993) and Witt (1993).

B1600+434 is another interesting gravitational mirage lensed by an edge-on disk galaxy. Koopmans & de Bruyn (2000) measured the radio time delay between the two images of the system and derived a radio difference light curve which is in disagreement with zero. They investigated both scintillation and microlensing as possible causes of the non-intrinsic radio variability. If microlensing is the origin of the "anomalous" difference light curve, then it could indicate the presence of a lens galaxy dark halo filled with MACHOs of mass  $\geq 0.5 M_{\odot}$ .

## 1.2 Microlensing in the first gravitational lens system (Q0957+561)

A third well-known microlensed quasar is the  $z = 1.41$  double system Q0957+561A,B. The main lens galaxy is an elliptical galaxy (cD) at  $z = 0.36$ . While the light associated with the image B crosses an internal region of the lens galaxy, the light path associated with the component A is  $\approx 5$  arcsec away from the centre of the galaxy. The cD galaxy is close to the centre of a galaxy cluster, and consequently, the normalized surface mass densities  $\kappa_A$  and  $\kappa_B$  are the projected mass densities of the lensing galaxy plus cluster along the lines of sight, normalized by the critical surface mass density. Pelt et al. (1998) used the recent values  $\kappa_A = 0.22$  and  $\kappa_B = 1.24$ , which originate from an extended galaxy halo consisting of the elliptical galaxy halo and an additional matter related to the cluster. It is possible that a considerable part of the extended halo mass does consist of a dark component, although an estimate of the stellar contribution (luminous stars) to  $\kappa_A$  and  $\kappa_B$  is not so easy as in the Milky Way. For the image B, if the fraction of mass in granular form  $\kappa_{BG}$  is dominated by normal stars and dark stars similar to the objects that have been discovered in the Galaxy (Alcock et al.

2000), and simultaneously, the main part of the halo mass is due to a smooth component ( $\kappa_{BG} \ll \kappa_B$ ,  $\kappa_{BG} \ll 1$ ) and the source quasar is small, then we must expect some long-timescale microlensing event caused by one star (luminous or dark) crossing the path of this image. In that case of small source/one star approximation, the timescale of an event will be  $t_o(\text{years}) \approx 17 \sqrt{M(M_{\odot})} [600/v_t(\text{km s}^{-1})]$ , where  $v_t$  is the transverse velocity, and the magnification of the B component has a typical duration of several years for a  $0.5\text{--}1 M_{\odot}$  star and any reasonable choice of  $v_t$ . When  $\kappa_{BG}$  is high ( $\kappa_{BG} \sim 1$ ) and/or the source is large, several stars at a time must be considered and the model by Chang & Refsdal (1984) is not suitable. The small source/one star model by Chang & Refsdal (1984) was generalized in the case of a small source and a large optical depth (Paczynski 1986) and the case of an extended source and an arbitrary optical depth (Kayser, Refsdal & Stabell 1986; Schneider & Weiss 1987; Wambsganss 1990). Therefore, the formalisms by Chang & Refsdal (1984), Paczynski (1986) and Wambsganss (1990) as well as new analytical approximations seem useful tools for a detailed analysis of the optical microlensing history of QSO 0957+561. A long-timescale microlensing signal was unambiguously observed from 1981 to 1999; see Pelt et al. (1998), Press & Rybicki (1998), Serra-Ricart et al. (1999, subsequently Paper I). In this paper, we concentrate on the possible rapid microlensing signal. In a forthcoming paper, we will carry out a comparison between the annual differences (averages from January to December)  $B - A$  and the predictions from different models and physical parameters.

In the past, using a record of brightness including photometric data (in the R band) up to 1995 and a time delay of 404 days, Schild (1996, hereafter S96) analyzed the possible existence of short-timescale microlensing (rapid external variability on a timescale of months) and very rapid microlensing events (with duration of  $\leq 3$  weeks) in the double QSO 0957+561A,B. He found numerous events with quarter-year and very short timescales (a few days). S96 also claimed that the slower component (events with a width of 90 days) can be interpreted as the imprint of an important population of microlenses with planetary mass of  $\sim 10^{-5} M_{\odot}$ . Assuming an improved delay value of 417 days, Goicoechea et al. (1998, subsequently G98) showed a difference light curve corresponding to the 1995/1996 seasons in Schild's dataset. G98 obtained fluctuations which could be associated with microlensing events, in fact, our results are in agreement with the existence of strong microlensing: the fluctuations in the difference light curve are clearly inconsistent with zero and similar to the fluctuations in the quasar signal. New work by Schild and collaborators pointed in the same direction: adopting a time delay of 416.3 days, Pelt et al. (1998) found that Schild's photometry shows evidence in favour of the presence of short-timescale microlensing; Schild (1999) made a wavelet exploration of the QSO 0957+561 brightness record, and reported that the rapid brightness fluctuations observed in the A and B quasar images (whose origin may be some kind of microlensing) are not dominated by observational noise; and Colley & Schild (1999), from a new reduction of "old" photometric data (subtracting out the lens galaxy's light according to the *HST* luminosity profile and removing cross talk light from the A and B images apertures), derived a structure function for variations in the R-band from lags of hours to years, a time delay of 417.4

days and a microlensing candidate on a timescale of a day, which could imply planetary MACHOs in the lens galaxy halo. So, from the photometry taken at Whipple Observatory 1.2 m telescope by Schild, one obtains two important conclusions. First, there is evidence in favor of the existence of true short-timescale microlensing signal. Second, this rapid signal seems to support the presence of MACHOs (in the halo of the cD galaxy) having a very small mass. However we note that Gould & Miralda-Escudé (1997) have introduced an alternative explanation to the possible rapid microlensing in the double QSO 0957+561A,B, which is related to hot spots or other moving structures in the accretion disk in the quasar, and so, planetary objects are not involved.

QSO 0957+561A,B was photometrically monitored at Apache Point Observatory (Kundić et al. 1995, 1997) in the g and r bands, during the 1995 and 1996 seasons. Schmidt & Wambsganss (1998, hereafter SW98) analyzed this photometry and searched for a microlensing signature. Considering the photometric data in the g band and a delay of 417 days, SW98 produced a difference light curve covering  $\approx 160$  days and concluded that it is consistent with zero. There is no variation in the difference light curve with an amplitude in excess of  $\pm 0.05$  mag and the total magnitude variation of a hypothetical microlensing signal is assumed to be less than 0.05 mag (see the dashed lines in Fig. 1 of SW98). They employed this last upper limit to obtain interesting information on the parameter pair MACHO-mass/quasar-size. The lack of observed fluctuations rules out a population of MACHOs with  $M \leq 10^{-3} M_{\odot}$  for a quasar size of  $10^{14}$  cm (25%-100% of the matter in compact dark objects). However, other possible scenarios (e.g., a small source and a halo consisting of MACHOs with  $M \geq 10^{-2} M_{\odot}$ , a source size of  $10^{15}$  cm and a halo with compact dark objects of mass  $\leq 10^{-3} M_{\odot}$ , etc.) cannot be ruled out from the bound on the microlensing variability in the 160 days difference light curve. In short, SW98 have not found reliable evidence for the presence of rapid microlensing events.

The gravitational lens system Q0957+561 was also monitored by our group with the IAC-80 telescope at Teide Observatory, from the beginning of 1996 February to 1998 July (see Paper I). We re-reduced our first 3 seasons (1996-1998) of QSO 0957+561 observations in the R band, made the difference light curves for 1996/1997 seasons and 1997/1998 seasons and studied the origin of the deviation between the light curves of the two images. All the results are presented in this article. The plan of the paper is as follows: in Sect. 2 we present the difference light curves and report on new constraints on microlensing variability. In Sect. 3 we suggest different models that explain the difference signal. In Sect. 4 we discuss the sensitivity of the telescope to different microlensing "peaks". At the end of the paper (Sect. 5), we summarize our results.

## 2 FIRST THREE SEASONS OF QSO 0957+561 OBSERVATIONS IN THE R BAND: DIFFERENCE LIGHT CURVES

We have been monitoring Q0957+561 over the past 4 years (from 1996 February) with the 82 cm IAC-80 telescope (at Teide Observatory, Instituto de Astrofísica de Canarias,

Spain) and have obtained a large R band dataset. The contribution to the solution of the old controversy regarding the value of the time delay ( $\approx 400$ -440 days or  $> 500$  days ?) was the first success of the monitoring program (Oscoz et al. 1996; see also Kundić et al. 1995, 1997; Oscoz et al. 1997).

In order to give refined measurements of both time delay and optical microlensing, we have introduced some modification with respect to the original aperture photometry (see Oscoz et al. 1996). Reduction of the images A and B is complicated by the presence of cross contamination and contamination from light of the main lensing galaxy. The two kinds of contamination depend on the seeing, and it is not clear what is the optimal way of obtaining the best photometric accuracy. At present, we reduce each available night by fitting a profile to the images, which is consistent with the point spread function of comparison stars. This new method of reduction and the photometry from 1996 to 1998 (the first 3 seasons) are detailed in Paper I. A table including all data is available at <http://www.iac.es/project/quasar/lens7.html>.

In the QSO 0957+561 quasar, a time delay of  $\approx 420$  days is strongly supported (e.g., G98). Using our first 3 seasons of data, the time delay estimates (in Paper I) are of  $425 \pm 4$  days (from the  $\delta^2$ -test, which is based on discrete correlation functions) and  $426 \pm 12$  days (from dispersion spectra). A comparison between the discrete cross-correlation function and the discrete autocorrelation function, indicates that a time delay of  $\leq 417$  days is in disagreement with the photometry (see Fig. 16 of Paper I), while a delay of about 425 days is favoured. Thus, we adopted a time delay of 425 days.

We concentrate now on the difference light curves. In order to estimate the difference light curve (DLC) for the 1996/1997 and the 1997/1998 seasons, we used 30 observations of image A corresponding to the 1996 season (A96), 28 observations of image B corresponding to the 1997 season (B97), 44 photometric data of image A in the 1997 season dataset (A97) and 84 photometric data of image B in the 1998 season dataset (B98). There are about 100 days of overlap between the time-shifted (in the time delay) light curve A96 and the light curve B97, and about 230 days of overlap between the time delay-corrected light curves A97 and B98. A main problem of the IAC-80 telescope (using the available observational time of 20-30 min/night) is related to the photometric errors. The mean errors in the initially selected datasets are approximately 19 mmag (A96), 24 mmag (B97), 28 mmag (A97) and 24 mmag (B98). For short-timescale microlensing studies, these errors are large and one must re-reduce the data (grouping them for obtaining lower errors). Because of the possible rapid microlensing variability on one month timescale, the timescale of the groups should not be too large ( $\leq 10$  days); it should not be too small for having a sufficient number of data, and so, relatively small errors. The re-reduced photometry consists of 12, 11, 22 and 36 "observations" in four new (and final) datasets A96, B97, A97 and B98, respectively. These datasets are available by sending a request to [rmerino@astro.physik.uni-potsdam.de](mailto:rmerino@astro.physik.uni-potsdam.de). For groups in A96, the timescales are less than 3 days and the mean error is of  $\approx 12$  mmag, for groups in B97, the timescales are  $\leq 8$  days and the mean uncertainty is of  $\approx 16$  mmag, for groups in A97, the timescales are also  $\leq 8$  days and the mean error is lowered to  $\approx 20$  mmag, and for groups

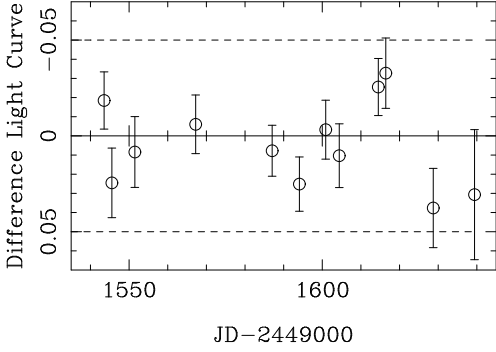


**Figure 1.** Difference light curve for 1996/1997 seasons (in the R band). We used bins with semi-size of 9 days and adopted a time delay of 425 days. The times associated with the circles are the dates in the time-delay shifted light curve *A96* (see main text).

in *B98*, the maximum timescale and the mean uncertainty are 6 days and 16 mmag, respectively. Therefore, making groups with a maximum timescale of  $\approx 1$  week (the mean timescale is of  $\approx 2$  days), the mean errors are lowered in 7-8 mmag.

As we have seen in the previous paragraph, the brightness record for the A image (*A96* or *A97*) is measured only at a set of discrete times  $t_i$  ( $i = 1, \dots, N$ ) and the light curve for the B image (*B97* or *B98*) is also determined at discrete times  $t_j$  ( $j = 1, \dots, M$ ). Since the observational light curves are irregularly sampled signals, to obtain the DLC (*A96/B97* or *A97/B98*), we can use different methodologies, for example, the interpolation suggested by SW98 or the binning that appears in G98. Here, we are interested in the DLC binned in intervals with size  $2\alpha$  around the dates in the light curve  $A^{TS}$  (time delay-shifted light curve *A*). In other words, each photometric measurement  $A_i^{TS}$  at the date  $t_i + \Delta\tau_{BA}$ , where  $\Delta\tau_{BA}$  is the time delay, will be compared to the observational data  $B_j^{MS} = B_j + \langle A \rangle - \langle B \rangle$  at  $t_i + \Delta\tau_{BA} - \alpha \leq t_j \leq t_i + \Delta\tau_{BA} + \alpha$  ( $B^{MS}$  is the magnitude-shifted light curve *B*). The values  $B_j^{MS}$  within each bin are averaged to give  $\langle B_j^{MS} \rangle_i$  ( $i = 1, \dots, N$ ), and one obtains the difference light curve (DLC)

$$\delta_i = \langle B_j^{MS} \rangle_i - A_i^{TS}, \quad (1)$$

being  $i = 1, \dots, N$ . The observational process  $A^{TS}(t)$  can be expanded as an intrinsic signal  $s(t)$  plus a noise process  $n_A(t)$  related to the procedure to obtain the measurements, and a microlensing signal  $m_A(t)$ . In a similar way,  $B^{MS}(t) = s(t) + n_B(t) + m_B(t)$ . So, the deviation  $\delta_i$  must be interpreted as a combination of several factors, i.e.,

$$\delta_i = [\langle s_j \rangle_i - s_i] + [\langle n_{Bj} \rangle_i - n_{Ai}] + [\langle m_{Bj} \rangle_i - m_{Ai}]. \quad (2)$$

If  $s(t)$  is a smooth function, then  $s_i = s(t_i)$  and  $s_j = s(t_j)$ , while when  $s(t)$  is a stochastic process,  $s_i$  represents a realization of the random variable  $s(t_i)$  and  $s_j$  denotes a realization of the random variable  $s(t_j)$ . With respect to the observational noise,  $n_{Ai}$  is a realization of the random variable  $n_A(t_i)$  [similarly,  $n_{Bj}$  is one of the possible values of  $n_B(t_j)$ ]. Also, in Eq. (2),  $m_{Ai} = m_A(t_i)$  and  $m_{Bj} = m_B(t_j)$ . From Eq. (2) it is inferred that the difference signal will be

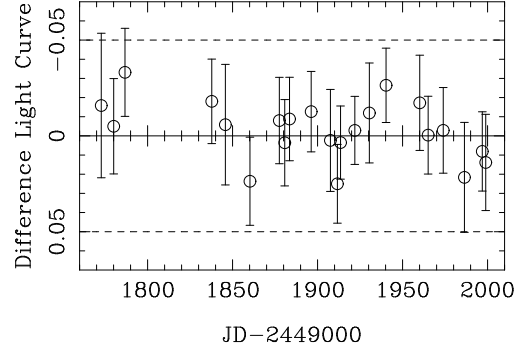


**Figure 2.** Difference light curve for 1997/1998 seasons (in the R band). We used bins with semi-size of 8 days and adopted a time delay of 425 days. The deviations  $[\delta_i]$  are evaluated at discrete dates corresponding to the time-delay shifted light curve *A97*.

never zero, even in absence of microlensing. There is a background dominated by observational noise, which is present in any realistic situation. In the case of very weak or null microlensing, we expect a trend of the DLC rather consistent with zero [taking into account the standard errors  $\epsilon_1, \dots, \epsilon_N$  in the deviations estimated from Eq. (1)]. However, in the case of strong microlensing, several absolute deviations  $|\delta_i|$  should be noticeably larger than the associated uncertainties  $\epsilon_i$ .

For the 1996/1997 seasons (from the final datasets *A96* and *B97*), using a time delay of 425 days and bins with semi-size of  $\alpha = 9$  days, we derived the DLC that appears in Fig. 1. Two thresholds are also illustrated:  $\pm 0.05$  mag (discontinuous lines). In Fig. 1, there is a "peak" around day 1615: two contiguous points significantly deviated from the zero line, that verify  $|\delta_i| > \epsilon_i$ . If the whole DLC is modelled as a single Gaussian event and the data are fitted to the model, we obtain that the amplitude and the full-width at one-tenth maximum (FWTM) of the Gaussian law must be  $\approx -33$  mmag and  $\approx 14$  days, respectively (best-fit characterized by  $\chi^2/N \approx 1$ ). Apart from this very short duration event, which is probably caused by observational noise (see next section), there is no evidence in favor of the existence of an event on longer timescales. We note that "event" is used in a general sense, and it may be due to true microlensing, observational noise, a combination of both or other mechanisms. In particular, none Schild-event (events having a width of three months and an amplitude of  $\pm 50$  mmag; see S96) is found. Although the difference signal is only tested during a 100 days period, to find a Schild-event belonging to a dense network of similar fluctuations (positive and negative), the "sampling" would be sufficient. In any case, from our second DLC (see here below), we must be able to confirm/reject the existence of a network of events with quarter-year timescale and an amplitude of  $\pm 50$  mmag. Finally, there are derived bounds on the amplitude of the microlensing fluctuations of  $\pm 0.05$  mag, which are similar to the bounds for 1995/1996 seasons (see Introduction and SW98).

For the 1997/1998 seasons (from the final datasets *A97* and *B98*), we also made the corresponding DLC. In Fig. 2,

the DLC and two relevant thresholds are depicted. The difference signal is in apparent agreement with zero, i.e., Fig. 2 shows a noisy relationship  $B^{MS} = A^{TS}$ . We observe no Schild-events, and therefore, *the total difference signal ( $\approx 1$  year of overlap between the time-shifted light curve for the A component and the magnitude-shifted light curve for the B component) is in clear disagreement with the claim that 90 days and  $\pm 50$  mmag fluctuations occur almost continuously*. One can also infer constraints on the microlensing variability. In good agreement with the DLCs for 1995-1997 seasons, a hypothetical microlensing signal cannot reach values out of the very conservative interval  $[-0.05 \text{ mag}, +0.05 \text{ mag}]$ . We finally remark that the methodology introduced by SW98 (the technique of interpolation) leads to DLCs similar to the DLCs discussed here (Figs. 1-2).

### 3 INTERPRETATION OF THE DIFFERENCE SIGNAL

The DLCs presented in Sect. 2 are in apparent agreement with the absence of microlensing signal. However, to settle some doubts on the ability of the observational noise in order to generate the observational features (e.g., the very rapid event in Fig. 1) and the measured variabilities (rms averages), a more detailed analysis is needed. In this section, we are going to test three simple pictures without microlensing. In brief, the ability of some models for generating combined photometries and difference signals similar to the observational ones is discussed in detail.

The observational combined photometry consists of both light curves  $A^{TS}$  and  $B^{MS}$ . Thus, assuming that  $m(t) = 0$ , the combined light curve (CLC) must be related to a process  $C(t) = s(t) + n(t)$ . The intrinsic signal  $s(t)$  is chosen to be either a smooth function (polynomial; picture I) or a polynomial plus a stationary noise process (picture II) or a correlated stationary process (picture III). In the first case (picture I), we work with  $s(t) = \sum_{p=0}^n a_p t^p$  (when the CLC is reasonably smooth, this intrinsic signal is a suitable choice). The polynomial law leads to  $C_k = \sum_{p=0}^n a_p t_k^p + n_k$  at a date  $t_k$ , where  $C_k$  ( $k = 1, \dots, N+M$ ) are the combined photometric data. Considering that the process  $n(t)$  is Gaussian with  $\langle n(t) \rangle = 0$  and  $\sigma_n^2(t) = \langle n^2(t) \rangle$ , and identifying the measurement errors  $\sigma_k^2$  with the noise process  $\sigma_n^2(t_k)$ , the probability distribution of  $n_k$  at a given time  $t_k$  is  $P_k(n_k, t_k) = (1/\sqrt{2\pi\sigma_k}) \exp(-n_k^2/2\sigma_k^2)$ . Here, the angle brackets denote statistical expectation values. As the random variables  $n(t_k)$ ,  $k = 1, \dots, N+M$ , are independent (the noise is uncorrelated with itself), the joint probability distribution of the noise vector  $\mathbf{n} = (n_1, \dots, n_{N+M})$  is given by

$$P(\mathbf{n}) = \prod_{k=1}^{N+M} P_k$$

$$= (2\pi)^{-\frac{N+M}{2}} \prod_{k=1}^{N+M} (1/\sigma_k) \exp\{-[C_k - \sum_{p=0}^n a_p t_k^p]^2 / 2\sigma_k^2\}. \quad (3)$$

Maximizing the likelihood function  $L = \ln P$  with respect to the parameters  $a_p$ , or equivalently, minimizing  $\chi^2 = \sum_{k=1}^{N+M} [C_k - \sum_{p=0}^n a_p t_k^p]^2 / \sigma_k^2$ , we find a possible reconstruction of the intrinsic signal (and thus, a model). If this procedure does not work (e.g.,  $\chi^2/dof$  is relatively large, with

$dof = N+M-(n+1)$  being the number of degrees of freedom), we perform a fit including a stationary intrinsic noise as an additional ingredient (picture II). This new ingredient can account for noisy CLCs. The intrinsic noise  $\eta(t)$  is taken to be Gaussian with  $\langle \eta(t) \rangle = 0$  and  $\sigma_\eta^2(t) = \sigma_{int}^2$ , and moreover,  $\eta(t)$  is uncorrelated with both  $n(t)$  and with itself. Now,  $C(t) = \hat{s}(t) + \xi(t)$ , where  $\hat{s}(t) = \sum_{p=0}^n a_p t^p$  and  $\xi(t) = n(t) + \eta(t)$ , and we focus on the global noise process  $\xi(t)$ . As the processes  $n(t)$  and  $\eta(t)$  are Gaussian and mutually independent, their sum is again Gaussian, and the average and variance of  $\xi(t)$  are the sums of the averages and variances of both individual noise processes. The probability distribution of  $\xi_k$  at an epoch  $t_k$  can be written as  $P_k(\xi_k, t_k) = [1/\sqrt{2\pi}(\sigma_k^2 + \sigma_{int}^2)^{1/2}] \exp[-\xi_k^2/2(\sigma_k^2 + \sigma_{int}^2)]$ , and the joint probability distribution of the noise vector  $\xi = (\xi_1, \dots, \xi_{N+M})$  should be  $P(\xi) = \prod_{k=1}^{N+M} P_k(\xi_k, t_k)$ . Finally, instead of the standard procedure (to maximize the likelihood function), we equivalently minimize the function

$$\hat{\chi}^2 = \sum_{k=1}^{N+M} \{\ln(\sigma_k^2 + \sigma_{int}^2) + [C_k - \sum_{p=0}^n a_p t_k^p]^2 / (\sigma_k^2 + \sigma_{int}^2)\}. \quad (4)$$

Through this method, the intrinsic signal is partially reconstructed. We find the coefficients of the polynomial and the variance of the intrinsic noise, but after the fit, the realizations  $\eta_k$  ( $k = 1, \dots, N+M$ ) remain unknown. However, the derived model permits us to make simulated CLCs and DLCs, since only the knowledge of the smooth intrinsic law and the statistical properties of the noise processes are required for this purpose.

A very different procedure was suggested by Press, Rybicki & Hewitt (1992 a,b, hereafter PRH92). They assumed the intrinsic signal as a correlated stationary process. For this case III, it is possible a reconstruction of the realizations of  $s(t)$ , provided that the correlation properties are known. PRH92 considered that the observational noise  $n(t)$  is uncorrelated with  $s(t)$  (and with itself), and therefore, only the autocorrelation function  $K_s(\tau) = \langle \tilde{s}(t)\tilde{s}(t+\tau) \rangle$  is needed, being  $\tilde{s}(t) = s(t) - \langle s \rangle$ . The autocorrelation function of the intrinsic signal is not known a priori and must be estimated through the CLC. We can relate the autocorrelation properties to the first-order structure function  $D_s^{(1)}(\tau)$  by

$$D_s^{(1)}(\tau) = (1/2\nu) \sum_{l,m} (s_m - s_l)^2$$

$$\approx \frac{1}{2} \langle [\tilde{s}(t+\tau) - \tilde{s}(t)]^2 \rangle = K_s(0) - K_s(\tau), \quad (5)$$

where the sum only includes the  $(l,m)$  pairs verifying that  $t_m - t_l \approx \tau$  (the number of such pairs is  $\nu$ ). From the CLC, one infers (e.g., Haarsma et al. 1997)

$$D_s^{(1)}(\tau) \approx (1/2\nu) \sum_{l,m} [(C_m - C_l)^2 - \sigma_l^2 - \sigma_m^2], \quad (6)$$

which is an evaluation of the difference  $K_s(0) - K_s(\tau)$ . As usual we assume a power-law form for the first-order structure function, and perform a fit to the power law. Finally, the variance of the intrinsic process  $K_s(0)$  is assumed to be the difference between the variance of the CLC and a correction due to the observational noise. The whole technique is described in PRH92 and other more recent papers (e.g., Haarsma et al. 1997).

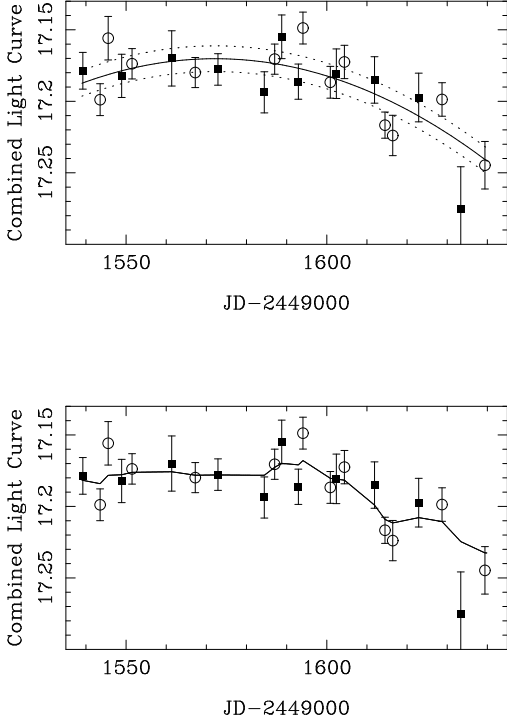


**Figure 3.** The combined photometry of QSO 0957+561A,B for the 1996/1997 seasons in the R band (at Teide Observatory). The open circles trace the time-shifted (+ 425 days) light curve *A96* and the filled squares trace the magnitude-shifted (+ 0.0658 mag) light curve *B97*. The lines are related to two reconstructions of the intrinsic signal: considering an intrinsic signal of the kind polynomial plus stationary noise (top panel) and the optimal reconstruction following the PRH92 method (bottom panel).

### 3.1 The 1996/1997 seasons

For the 1996/1997 seasons, we first have done the corresponding CLC. In a second step, using the picture I (see above), we attempted to fit the combined photometry. A quadratic law ( $n = 2$ ) gives  $\chi^2/dof = 1.65$  (best fit), whereas  $\chi^2/dof(n = 1) = 2.52$ ,  $\chi^2/dof(n = 3) = 1.74$  and  $\chi^2/dof(n = 4) = 1.83$ . Thus the modelling of the CLC has proven to be some difficult. Fortunately, the inclusion of an intrinsic noise (picture II) with moderate variance does not fail to generate an acceptable fit. When the intrinsic signal is the previous best quadratic fit to which an intrinsic noise with  $\sigma_{int} = 9$  mmag is added, we obtain  $\chi^2/dof = 1.15$  ( $\chi^2/N+M = 0.95$ ). The quality of the fit has changed significantly with the addition of the new noise, whose variance ( $\sigma_{int} = 9$  mmag) is less than the mean variance of the observational noise (= 12-16 mmag). In Fig. 3 (top panel) the CLC and the reconstruction are presented. The open circles represent the time-shifted light curve *A96*, while the filled squares are the magnitude-shifted light curve *B97*. The best polynomial ( $n = 2$ ) is traced by means of a solid line, and the two lines with points are drawn at  $\pm 9$  mmag (the best value of  $\sigma_{int}$ ) from the polynomial. Apart from the CLC, we checked the observational structure functions  $D_s^{(1)}$  [see Eq. (6)] and  $D_s^{(2)}$  as well as the predictions (with respect

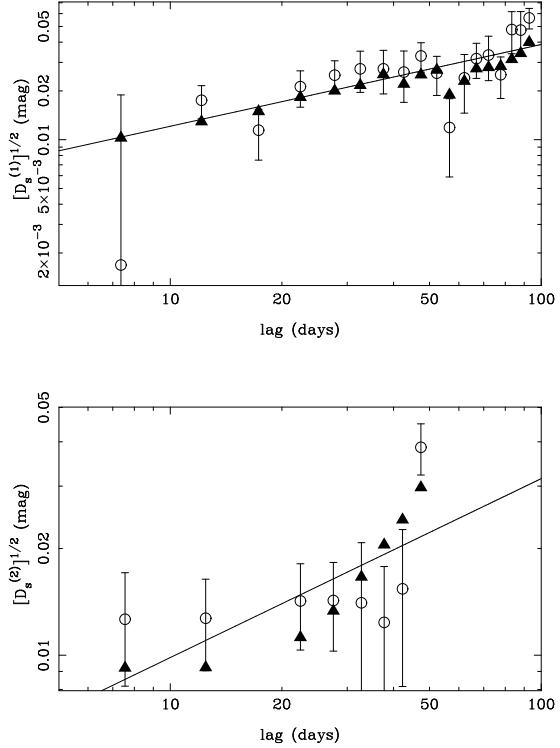


**Figure 4.** The first-order and second-order structure functions (1996/1997 seasons in the R band). The open circles are the values inferred from the observational data and the filled triangles are the predictions from the reconstruction of the kind polynomial + stationary noise. The observational first-order structure function was fitted to a power-law  $E\tau^\epsilon$  (solid line in the top panel). Assuming this fit as an estimation of the autocorrelation properties of a hypothetical correlated stationary process ( $K_s(0) - K_s(\tau)$ ), the predicted second-order structure function is illustrated by a solid line in the bottom panel.

to the structure functions) from our first successful reconstruction. The observational second-order structure function is computed in the following way (see Simonetti, Cordes & Heeschen 1985; we take a normalization factor equal to 1/6):

$$D_s^{(2)}(\tau) \approx (1/6\mu) \sum_{l,m,n} [(C_n - 2C_m + C_l)^2 - \sigma_l^2 - 4\sigma_m^2 - \sigma_n^2], \quad (7)$$

where  $\mu$  is the number of  $(l,m,n)$  valid triads so that  $t_m - t_l \approx \tau$  and  $t_n - t_l \approx 2\tau$ . Also, the predicted structure functions are

$$D_s^{(1)}(\tau) \approx (1/2\nu) \sum_{l,m} [\hat{s}(t_m) - \hat{s}(t_l)]^2 + \sigma_{int}^2, \\ D_s^{(2)}(\tau) \approx (1/6\mu) \sum_{l,m,n} [\hat{s}(t_n) - 2\hat{s}(t_m) + \hat{s}(t_l)]^2 + \sigma_{int}^2, \quad (8)$$

being  $\hat{s}(t)$  the fitted quadratic law. Fig. 4 shows the good agreement between the observational values (open circles) and the predicted trends (filled triangles). This result confirms that the reconstruction is reliable. The meaning of the two straight lines in Fig. 4 will be explained here below.

Our interest in this paper is less directly in the details of a given reconstruction of the underlying intrinsic

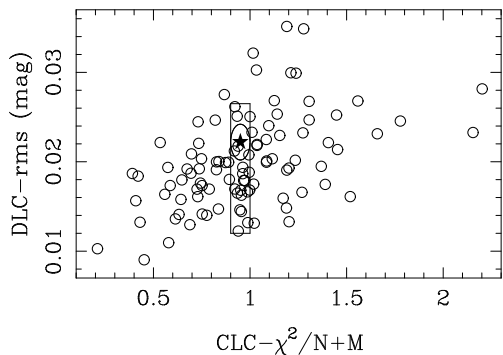


**Figure 5.** Global properties of the measured photometry for 1996/1997 seasons (filled star) and 100 simulated photometries (open circles). The numerical simulations arise from M1, which is a model with three ingredients: polynomial law + intrinsic noise + observational noise.

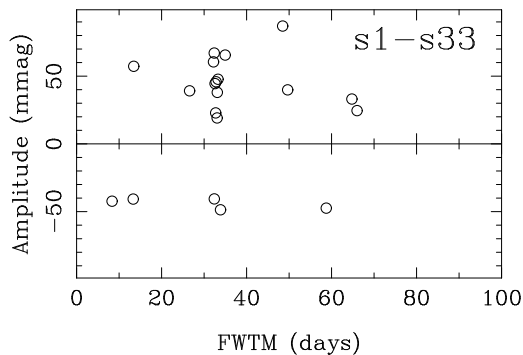


**Figure 7.** Gaussian events (they are classified according to their amplitude and FWTM) found in the first 33 simulations via M1. The number of features as well as the amplitudes and time-scales are relatively surprising.

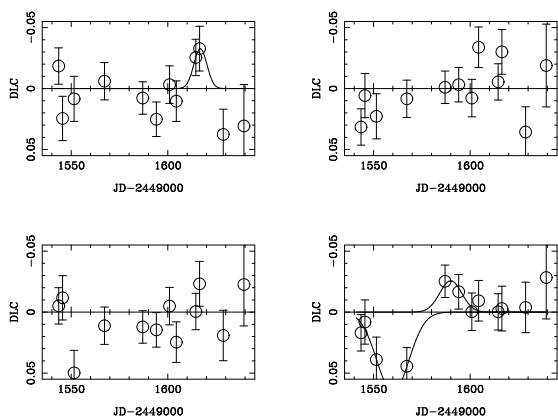


**Figure 6.** The true DLC for 1996/1997 seasons (left-hand top panel) together with 3 simulated DLCs (via M1). The solid lines are fits to Gaussian events. A curious result observed in the simulated DLCs is the existence of events, which could be naively interpreted as microlensing fluctuations.

signal than it is in analyzing simulated photometries consistent with the reconstruction and with the same sampling (dates) and errors as the measured data. The first model (M1) comprises the best quadratic fit in the absence of intrinsic noise (a smooth component) and a Gaussian noise process characterized by a known variance at discrete times  $t_k$ :  $\sigma_k^2 + \sigma_{int}^2$ . From M1 we derived 100 simulated CLCs and the corresponding DLCs. We remark that, in each simulation (CLC),  $N$  simulated data points represent a synthetic light curve  $A^{TS}$ , while the other  $M$  data are simulated measurements of the magnitude-shifted light curve  $B$ . Fig. 5 shows the relationship between the values of  $\chi^2/N+M$  ( $\chi^2 = \sum_{k=1}^{N+M} [C_k - \hat{s}(t_k)]^2 / [\sigma_k^2 + \sigma_{int}^2]$ ) and the rms averages of the DLCs ( $rms = [\frac{1}{N} \sum_{i=1}^N \delta_i^2]^{1/2}$ ). The 100 open circles are associated with the simulated photometries and the filled star is related to the measured photometry. The true (measured) photometry appears as a typical result of

the model. One sees in the figure a broad range for  $CLC-\chi^2/N+M$  (0.2-2.2) and  $DLC-rms$  (8-36 mmag), and the true values of  $CLC-\chi^2/N+M = 0.95$  and  $DLC-rms = 22$  mmag are well placed close to the centre of the open circle distribution. Thus, the measured combined photometry seems a natural consequence of M1, which is a model without very rapid and rapid microlensing. However, due to the event found in Fig. 1 (around day 1615) and other local features less prominent than the event, we would be to doubt this conclusion and to study details in the synthetic DLCs. In Fig. 5, to provide some guidance, the open circles corresponding to simulated datasets with  $CLC-\chi^2/N+M$  similar to the measured value have been enclosed in a rectangular box. Also, we have drawn an elliptical surface centred on the filled star, which includes (totally or partially) three open circles associated with the synthetic photometries analogous (global properties of both the CLC and the DLC) to the true brightness record. As we must put into perspective the very rapid event and other local properties discovered in the true DLC for 1996/1997 seasons, this DLC and its features were compared with the three DLCs that arise from the simulations. In Fig. 6 we present the comparison. All events (each event includes a set of two or more consecutive deviations which have equal sign and are not consistent with zero) has been fitted to a Gaussian law and marked in the figure. The measured DLC (left-hand top panel and Fig. 1) is not different to the other three. In fact, in our 100<sup>th</sup> simulation (s100; right-hand bottom panel), two events appear. The positive event is more prominent than the negative event, and this last one is similar to the measured one. With respect to the regions without events, the true variability cannot be distinguished from the simulated ones. To throw more light upon the problem, we searched for Gaussian events in 1/3 of all simulations (s1-s33), as a sample of the whole set of simulations because the computation turned out to be very time-consuming. The results are plotted in Fig. 7: amplitude of each event (mmag) vs. FWTM (days). There are a lot of events with amplitude in the interval [- 50 mmag, + 90 mmag] and duration < 70 days. In particular, the probability of observing a negative event is of 15% and the prob-

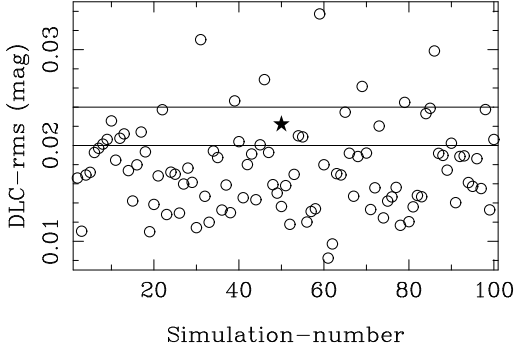


**Figure 8.** Global properties of the true DLC for 1996/1997 seasons (filled star) and 100 simulated DLCs (open circles). The numerical simulations were made through a model including the optimal reconstruction of a correlated stationary process and a Gaussian observational noise process whose variance at the dates of the real data is known.

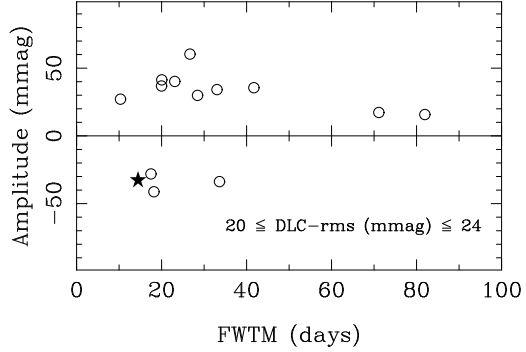


**Figure 10.** Gaussian events found in the numerical simulations (via M2) with  $20 \leq \text{rms (mmag)} \leq 24$  (open circles). Events very similar to the real event (filled star) are produced in two simulations.

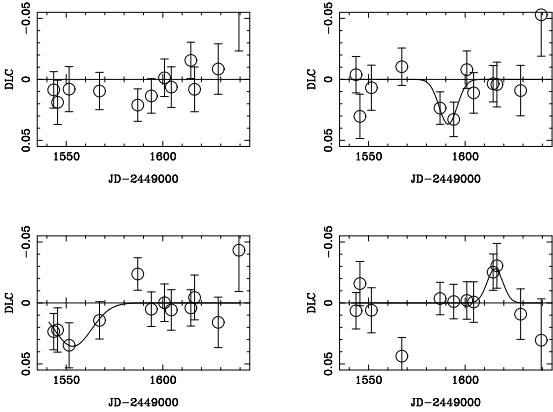


**Figure 9.** Four simulated DLCs (via M2). For comparison with the true event in Fig. 1 (see also Fig. 6), the Gaussian events have been clearly marked on the panels.

ability of observing one or more events is of about 50%. So, it must be concluded that *the noisy (around zero) difference light curve based on observations is totally consistent with M1, and the deviations from the zero line can be caused by the combined effect of the processes  $n(t)$  (main contribution) and  $\eta(t)$ .*

We also propose a reconstruction of the underlying intrinsic signal as realizations of a correlated stationary process (picture III). The observational first-order structure function can be fitted to a power-law  $E\tau^\epsilon$  (see Fig. 4, solid line in the top panel). If one considers this fit as an estimate of the difference  $K_s(0) - K_s(\tau)$  for a correlated stationary process, then it is straightforward to obtain the predicted second-order structure function (see Fig. 4, solid line in the bottom panel: the prediction is irrelevant to reconstruct the intrinsic signal, but it is necessary for testing the consistency of the starting point  $K_s(0) - K_s(\tau) = E\tau^\epsilon$ ) and to apply the reconstruction formalism by PRH92. Therefore,

we are able to find the realizations of the intrinsic process at the observational times  $t_k$  ( $k = 1, \dots, N+M$ ) as well as in the gaps between the observations. The PRH92 technique leads to an acceptable fit with  $\chi^2/dof = 1.18$  ( $dof = N+M-1$ ), and our second successful reconstruction is showed in Fig. 3 (bottom panel). The knowledge of both the optimal reconstruction and the properties of the Gaussian observational noise process at discrete times  $t_k$  ( $k = 1, \dots, N+M$ ), permits us to make 100 new simulations. In Fig. 8 details of the rms averages of the DLCs are provided (open circles). The observational DLC has a rms average (filled star) similar to the rms average of about 1/5 (20%) of the simulated DLCs. Furthermore, four simulated DLCs with rms in the interval  $[20 \text{ mmag}, 24 \text{ mmag}]$  (in Fig. 8, this range of variability is labeled with two horizontal lines) appear in Fig. 9. From the new model (M2), DLCs with no events (as in the analysis presented above, the Gaussian events are related to "peaks", or in other words, we only made events around consecutive multiple deviations with equal sign and well separate from zero) and DLCs that incorporate more or less prominent features are derived. We note that one DLC (right-hand bottom panel) has an event almost identical to the true one in Fig. 1 and Fig. 6. Fig. 10 shows the properties of all Gaussian events in the simulated DLCs with rms in the vicinity of the observational rms (open circles). The measured event is also depicted (filled star), and we can see two simulated events analogous to it. We finally conclude that *the observational DLC is in clear agreement with M2, and so, microlensing would be not advocated. In this framework (M2), the observational noise process is a sufficient mechanism for originating the measured deviations.*

### 3.2 The 1997/1998 seasons

The combined photometry for 1997/1998 seasons and the reconstruction based on a polynomial fit are showed in Fig. 11 (top panel). The open circles represent the time-shifted light curve A97 and the filled squares are the magnitude-shifted brightness record B98. There is no need for the presence of an intrinsic noise, and a simple quadratic law works well,



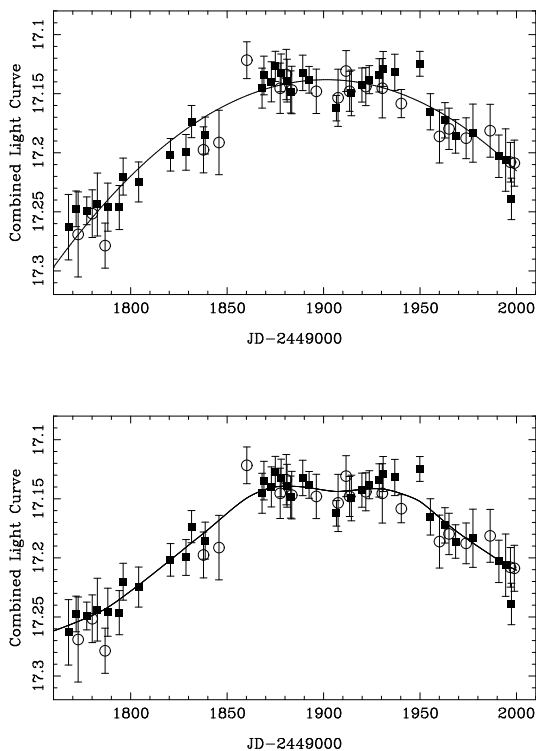


**Figure 11.** The combined photometry for 1997/1998 seasons in the R band (at Teide Observatory). The open circles trace the time-shifted (+ 425 days) light curve *A97* and the filled squares trace the magnitude-shifted (+ 0.0603 mag) light curve *B98*. The solid lines represent two reconstructions of the intrinsic signal: the best quadratic fit (top panel) and the optimal reconstruction following the PRH92 method (bottom panel).

leading to  $\chi^2/dof = 0.85$  (best fit). In Fig. 11 (top panel), the solid line traces the reconstruction of the intrinsic signal. Besides the comparison between the measured CLC and the fitted polynomial, we tested the predicted structure functions. In Fig. 12 we present the observational  $D_s^{(1)}$  and  $D_s^{(2)}$  [open circles; see Eqs. (6-7)] and the predictions from the best quadratic fit (filled triangles; see Eqs. (8) with  $\sigma_{int} = 0$ ). The laws traced by the dashed and solid lines in this figure will be discussed below. It is evident that the behaviours deduced from observations and the predicted trends agree very well, and this result indicates that the reconstruction is robust.

The first model for 1997/1998 seasons (M3) consists of the best quadratic fit together with a Gaussian observational noise process (whose variance is  $\sigma_k^2$  at discrete times  $t_k$ ,  $k = 1, \dots, N+M$ , being  $\sigma_k$  the measurement errors at the dates of observation  $t_k$ ). Using M3 we performed 100 simulated CLCs (and consequently, 100 simulated DLCs). The global properties of the simulated photometries (open circles) and the true dataset (filled star) are depicted in Fig. 13. If we concentrate on the simulations with  $\chi^2/N+M$  similar to the measured value (rectangular box), the true DLC has a rms relatively small (of about 15 mmag), but consistent with the rms distribution associated with the simulated DLCs. We remark that 3 simulations (open circles in the ellipti-

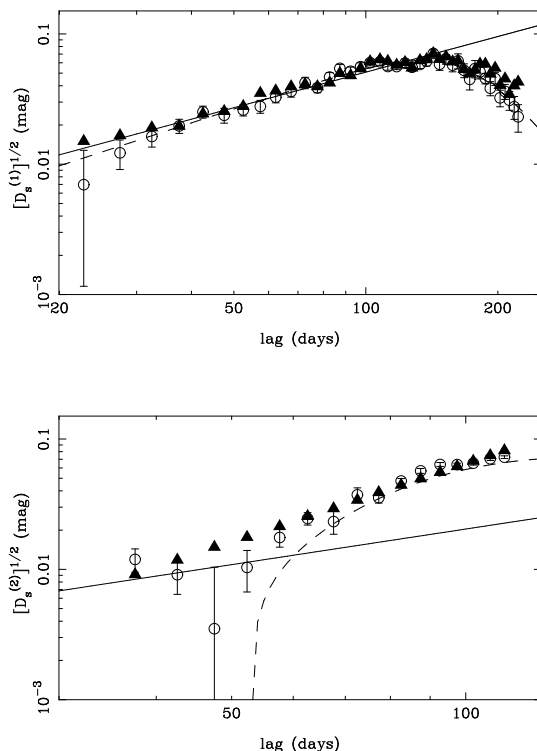


**Figure 12.** The first-order and second-order structure functions (1997/1998 seasons in the R band). The open circles are the values inferred from the observational data and the filled triangles are the predictions from the reconstruction of the kind polynomial. The observational first-order structure function was fitted to different laws, and two "reasonable" fits are drawn in the top panel (dashed and solid lines). If the fits are interpreted as the difference  $K_s(0) - K_s(\tau)$  for a correlated stationary process, the corresponding predicted second-order structure functions are illustrated by two lines in the bottom panel.

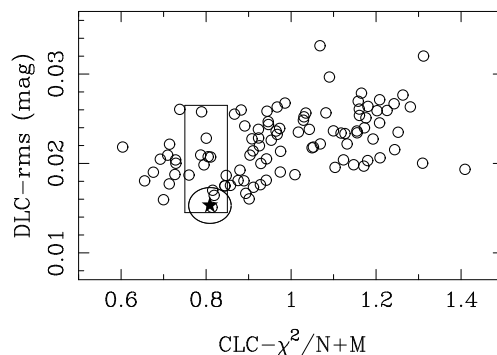


**Figure 13.** Global properties of the true photometry for 1997/1998 seasons (filled star) and 100 simulated photometries (open circles). The numerical simulations are based on a model of the kind polynomial plus observational noise.

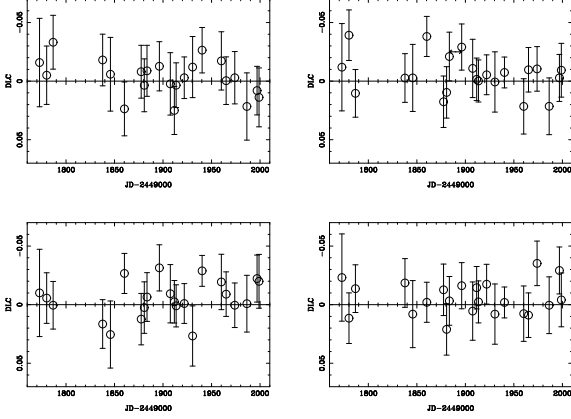


**Figure 14.** The true DLC for 1997/1998 seasons (left-hand top panel) together with 3 simulated DLCs (via M3). An only "peak" is marked by a double arrow (see right-hand top panel).

cal surface around the filled star) are analogous to the real brightness record, and in Fig. 14, their DLCs can be compared with the true DLC. The measured difference signal (left-hand top panel and Fig. 2) is a quasi-featureless trend and similar to the other synthetic DLCs. There are no significant events in these four DLCs with small global variability. We conclude that *a model with no microlensing (M3) has the ability of generating light curves like the real data for 1997/1998 seasons.* Henceforth, we are going to treat the "peaks" as top-hat fluctuations, i.e., given a "peak" including deviations  $\delta_{P1}, \dots, \delta_{PP}$  at times  $t_{P1}, \dots, t_{PP}$ , the amplitude and duration of the associated top-hat profile will be evaluated as the average of the individual deviations and the difference  $t_{PP} - t_{P1}$ , respectively. In Fig. 14, a "peak" (defined by two contiguous negative deviations, which are inconsistent with zero) appears in the DLC from the 7<sup>th</sup> simulation (s7; right-hand top panel). The "peak" is marked by a double arrow that represents the amplitude and duration of the associated top-hat profile.

The inspection of the observational first-order structure function (see Fig. 12) suggests that the underlying law could be intricate. To find the autocorrelation properties of a possible and plausible correlated stationary process causing the main part of the observed signal (picture III), this observational structure function was firstly fitted to a non-standard law  $D_s^{(1)}(\tau) = E\tau^\epsilon / [1 + (\tau/T)^\lambda]^2$ . As showed in Fig. 12 (dashed line in the top panel), the fit is excellent. However, when we attempt to reproduce the observational second-order structure function, an inconsistent prediction is derived (dashed line in the bottom panel). The prediction fails at  $\tau < 70$  days. Other functions led to fits more or less successful, and finally we adopted the point of view by PRH92. In Fig. 12 (top panel) one sees a power-law behaviour up to  $\tau = 140$  days. The drop at the largest lags is due to the coincidence of values in the starting and ending parts of the measured CLC. Therefore, we assume that the observational first-order structure function is a reliable estimator of  $K_s(0) - K_s(\tau)$  at  $\tau \leq 140$  days, whereas it is a biased estimator at  $\tau > 140$  days. The power-law fit to the data at lags  $\tau \leq 140$  days gives the autocorrelation properties for the correlated stationary process, shown as a solid

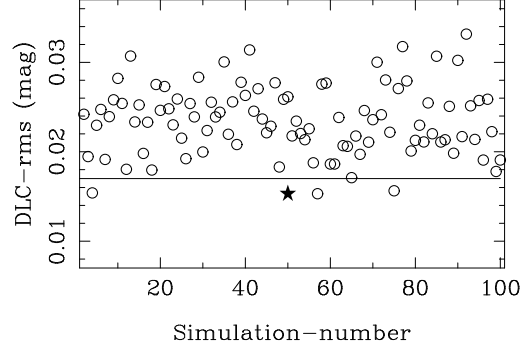


**Figure 15.** Global properties of the true DLC for 1997/1998 seasons (filled star) and 100 simulated DLCs (open circles). The numerical simulations were made from M4 (see main text).

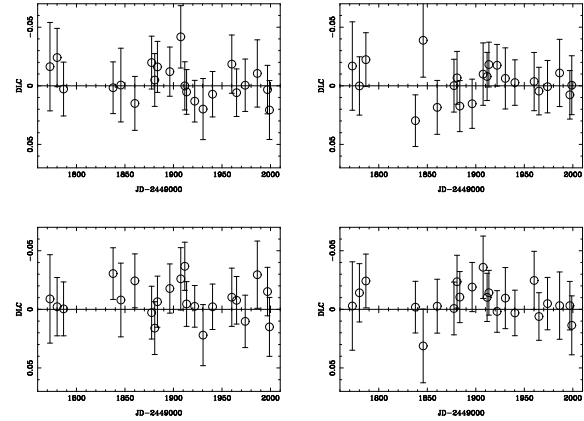


**Figure 16.** Four simulated DLCs via M4. No events are found (for a comparison, see Fig. 2).

line in the Fig. 12 (top panel). The predicted second-order structure function (Fig. 12, solid line in the bottom panel) is consistent with the observational one up to a lag of 70 days, and it deviates from the observational trend at  $\tau > 70$  days. However, since the observational second-order structure function at lag  $\tau$  is associated with the autocorrelation at lag  $2\tau$ , the observational  $D_s^{(2)}(\tau > 70$  days) will be related to the autocorrelation at  $\tau > 140$  days, which is poorly traced from observations. Thus the deviation at largest lags is reasonable and the global prediction should be considered as a consistent result.

Once the relationship between the structure function and the autocorrelation has been established, we can directly obtain both an optimal reconstruction of the realizations of the intrinsic signal and a new model (M4). The relatively smooth reconstruction is showed in Fig. 11 (bottom panel; the  $\chi^2/dof$  value is of 0.86), and the associated model leads to 100 simulations, whose global properties (rms averages of the DLCs) are presented in Fig. 15 (open circles). In Fig. 15, a filled star represents the true rms average, which is consistent (although marginally) with the rms distribution from simulations. Finally, four simulated DLCs with rms  $\leq$

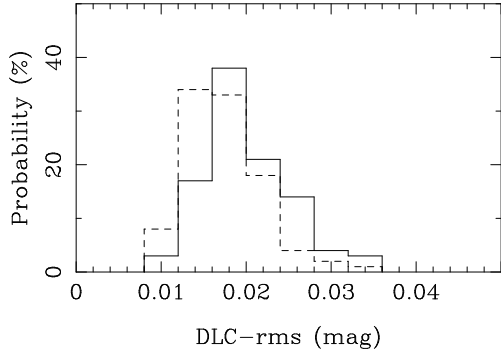


**Figure 17.** Probability distributions of the rms averages of the synthetic DLCs. The numerical simulations were made from M1 (solid line) and M2 (dashed line).

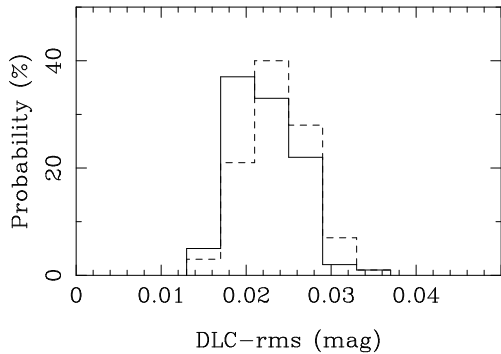


**Figure 18.** Probability distributions of the rms averages of the synthetic DLCs. The numerical simulations are based on M3 (solid line) and M4 (dashed line).

17 mmag (in Fig. 15, the upper limit of 17 mmag is marked with one horizontal line) have been selected for a more detailed inspection. We found noisy behaviours around zero and no events in these synthetic DLCs, i.e., the results agree with the analysis of the real difference signal for 1997/1998 seasons. The 4 quasi-featureless simulated DLCs appear in Fig. 16. We again showed that *microlensing is not necessary*. *The real combined photometry and difference signal can be due to a set of realizations of two very different processes: a correlated stationary process (intrinsic) and a Gaussian noise (observational)*.

#### 4 THE ABILITY OF THE IAC-80 TELESCOPE TO DETECT MICROLENSING "PEAKS"

The sensitivity of our telescope to microlensing variability in a given observational DLC is an important issue which merits more attention. To explain the observations for 1996/1997 seasons and 1997/1998 seasons, we proposed (in Sect. 3) four models based on pictures including only an in-

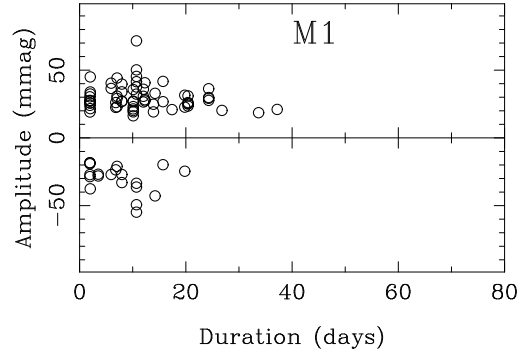


**Figure 19.** Top-hat fluctuations found in the numerical simulations based on M1. We show 84 features that appear in 100 simulated DLCs.

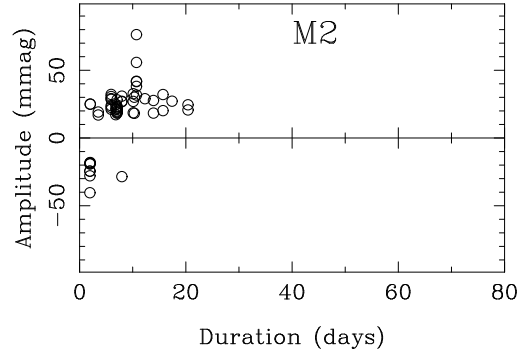


**Figure 20.** Top-hat fluctuations in 100 simulated (via M2) DLCs. They were found 55 "peaks".

trinsic signal and observational noise. The simulations arising from these models (100 simulated difference light curves per model) are a useful tool to study the statistical properties of the expected difference signal in the absence of microlensing, and so, to test the resolution of the IAC-80 telescope for microlensing variability. In Fig. 17 we present the probability distributions of the rms values (DLCs) derived from M1 (solid line) and M2 (dashed line). A value of about 20 mmag has a relatively high probability of 20-40%, while a rms exceeding 36 mmag is inconsistent with both models, as can be seen in Fig. 17. Fig. 18 also shows the probability of observing (in the absence of microlensing) different rms values: via M3 (solid line) and via M4 (dashed line). The rms averages in the interval 19-27 mmag are highly probable (20-40%), but a global variability characterized by either rms  $\leq 12$  mmag or rms  $\geq 38$  mmag can be excluded. As a general conclusion, the rms of the difference signal induced by noise does not exceed a threshold of 37 mmag. Therefore, *the rms values of future observational DLCs can be used to discriminate between the presence of the expected background (global variability with rms  $< 40$  mmag) and the probable existence of true microlensing signal (rms  $\geq 40$  mmag)*.

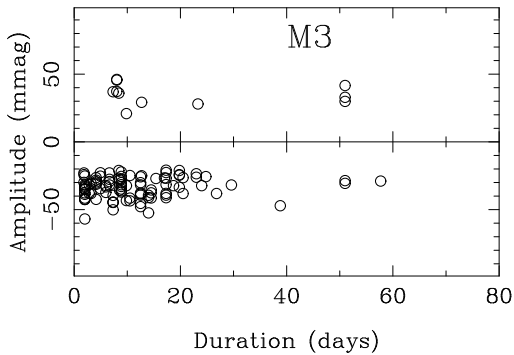


**Figure 21.** Top-hat fluctuations from M3. We note the existence of noise “peaks” with a duration longer than 40 days. All these features are however associated with an unfortunate small gap in our photometry.

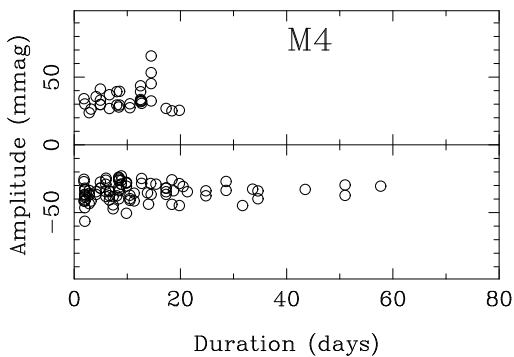


**Figure 22.** “Peaks” from M4.

The previous discussion on the global variability is interesting, but it is not the main goal of this section. Our main goal lies in discussing the sensitivity of the telescope (taking into account typical sampling, photometric errors, re-reduction and making of bins) to several classes of microlensing “peaks” (the cores of the microlensing events). We have seen, in Sect. 3, a figure that shows the properties of the Gaussian events (amplitude and FWTM) found in a subset of simulations from M1 (see Fig. 7). Fig. 7 can be compared to the distribution of top-hat fluctuations found in all DLCs generated with M1. In Fig. 19 the distribution of the top-hat fluctuations (basically the properties of the “peaks” associated with them) appears, and a direct comparison between Fig. 7 and Fig. 19 indicates the logical fact that Gaussian fits lead to longer durations than top-hat estimates. In the case of Gaussian fits, events with a duration (FWTM) of 1-2 months are abundant and only features with a timescale  $> 70$  days are ruled out. However, the “peaks” (from M1) with a timescale of about one month are scarce. To discuss the power of resolution of the telescope for local microlensing variability we chose the top-hat fluctuations (“peaks”) instead of the events. The properties of

an event (around a “peak”) depend on the assumed profile (e.g., Gaussian, Lorentzian, etc.) and the global behaviour of the DLC, whereas the top-hat shape directly traces the “peaks”, avoiding to make assumptions on their wings and the use of the rest of the corresponding DLCs. In a few words, the top-hat structures are more local and free from assumptions than the events.

The “peaks” from M2 (Fig. 20) are not so numerous as the top-hat fluctuations inferred from the first model (M1). Moreover, the new cloud of points (open circles) is more concentrated towards shorter durations. In fact, all “peaks” have a timescale of  $\leq 20$  days. When one takes M3 (Fig. 21) and M4 (Fig. 22) the situation is also somewhat different. The probability of observing a 40-60 days top-hat fluctuation is now of about 5%, although most features are due to a small gap of about 50 days around day 1815 (see Paper I and Fig. 2). Finally, Figs. 19-22 inform on the true ability of the IAC-80 telescope to detect microlensing fluctuations in an observational DLC free from gaps: a “peak” with a timescale  $> 40$  days should be interpreted as a feature related to microlensing or other mechanisms different to the observational noise, while as mainly caused by the poor resolution at the expected amplitudes within the interval  $[-50 \text{ mmag}, +50 \text{ mmag}]$ , the  $\leq 20$  days microlensing “peaks” cannot be resolved. Even in the unlikely case of very short-timescale microlensing signal with high amplitude, due to the smoothing by both the re-reduction and the binning as well as the current uncertainty of one week in the true time delay, it would be not possible to reliably reconstruct the microlensing “peaks”.

## 5 CONCLUSIONS

Several  $\sim 1$  metre class telescopes around the world are at present involved in different optical monitoring programs of quasars with the goal to detect microlensing. There are at least two “modest” telescopes searching for microlensing signal related to a far elliptical galaxy (which is responsible, in part, for the gravitational mirage Q0957+561). The data taken at Whipple Observatory 1.2 m telescope and at Teide Observatory IAC-80 telescope together with the photometry from a 3.5 m telescope (at Apache Point Observatory) represent a great effort in order to obtain an accurate time delay in Q0957+561, follow the long-timescale microlensing event in that system and find some evidence in favour of very rapid and rapid microlensing (Kundić et al. 1995, 1997; Oscoz et al. 1996, 1997; Pijpers 1997; Schild & Thomson 1997; Paper I; S96; Pelt et al. 1998; SW98; G98).

With respect to the very rapid (events with a timescale  $\leq 3$  weeks) and rapid (events with a duration of 1-4 months) microlensing, the previous results (before this article) are puzzling. The combined photometries (CLCs) from data taken at Whipple Observatory only can be well explained in the context of a picture including intrinsic variability, observational noise and microlensing variability on different timescales: from days to months (e.g., S96). The long-timescale microlensing does not play any role in a CLC. In particular, S96 reported on the existence of a network of rapid events with a few months timescale and an amplitude of about  $\pm 50$  mmag (these features found by Schild are called Schild-events). However, SW98 concluded that a pic-

ture with intrinsic signal and observational noise (without any need to introduce very rapid and rapid microlensing) is consistent with the observations at Apache Point Observatory. SW98 really show a difference light curve in global agreement with the zero line, but some doubt remains on the ability of the observational noise for producing the negative and positive measured events around "peaks" (a "peak" is constituted by a set of two or more consecutive deviations which have equal sign and are not consistent with zero). In any case, SW98 observed no Schild-events.

In this paper, motivated by the mentioned intriguing results on microlensing variability, we analyzed the data from our initial monitoring program with the IAC-80 telescope (see Paper I). We focused on the possible presence of rapid microlensing events in the light curves of QSO 0957+561 and the sensitivity of the telescope (using typical observational and analysis procedures) to microlensing "peaks". Our conclusions are:

(i) Using photometric data (in the R band) for the 1996-1998 seasons, we made two difference light curves (DLCs). The total difference signal, which is based on  $\sim 1$  year of overlap between the time-shifted light curve for the A component and the magnitude-shifted light curve for the B component, is in apparent agreement with the absence of microlensing signal. We can reject the existence (in our DLCs) of events with quarter-year timescale and an amplitude of  $\pm 50$  mmag, and therefore, Schild-events cannot occur almost continuously. On the contrary, they must be either rare phenomena (originated by microlensing or another physical process) or, because two observatories (Apache Point Observatory and Teide Observatory) found no Schild-events, untrue fluctuations associated with the observational procedure and/or the reduction of data at Whipple Observatory.

(ii) From a very conservative point of view, in our data, the amplitude of any hypothetical microlensing signal should be in the interval  $[-50 \text{ mmag}, +50 \text{ mmag}]$ . The rms averages of the DLCs (global variability) are of about 22 mmag (1996/1997 seasons) and 15 mmag (1997/1998 seasons), and reasonable constraints on the possible microlensing variability lead to interesting information on the granularity of the dark matter in the main lensing galaxy (a cD elliptical galaxy) and the size of the source (QSO). Thus the set of bounds derived from 1995-1998 seasons (SW98 and this work) rules out an important population of MACHOs with substellar mass for a small quasar size (Schmidt 1999).

(iii) In order to settle any doubt on the ability of the observational noise for generating the global (rms averages) and local (events and other less prominent features) properties of the DLCs, we have also carried out several experiments as "Devil's advocates". The measured variability (the rms value, a very rapid event and some minor deviations) in the DLC for 1996/1997 seasons can be caused, in a natural way, by the observational noise process. In the absence of microlensing signal, we proposed two different models (M1 and M2; see subsection 3.1) whose associated photometries (simulations) are consistent with the observations. In addition, the DLC for 1997/1998 seasons is a quasi-featureless trend with relatively small rms average. To explain the variability in our second observational DLC, we again showed that microlensing is not necessary. Two new models (M3 and M4; see subsection 3.2) only including the reconstruc-

tion of the intrinsic signal (assumed as a polynomial or a correlated stationary process) and a Gaussian observational noise process, led to simulated DLCs in agreement with the measured behaviour.

(iv) We finally show that from a typical monitoring with our telescope (observing times, method of analysis, etc.) is not possible the resolution of  $\leq 20$  days microlensing "peaks". The confusion with noise does not permit the separation between true microlensing features and "peaks" due to the observational noise. However, all hypothetical "peaks" with a timescale  $> 40$  days must be interpreted as phenomena which are not associated with the observational noise (e.g., microlensing fluctuations). At intermediate timescales (of about one month) the situation is somewhat intricate. Given a measured DLC, the probability of observing one noise "peak" (with a duration of about 30 days) is less than 10%. Therefore, if we search for microlensing signal and find an "intermediate peak", the relative probabilities that the fluctuation is a noise feature or a microlensing "peak" are  $< 1:10$ .

## ACKNOWLEDGMENTS

We are especially grateful to Joachim Wambsganss and Robert Schmidt for helpful discussions and comments on a first version of the paper. This work was supported by the P6/88 project of the Instituto de Astrofísica de Canarias (IAC), Universidad de Cantabria funds, and DGSIC (Spain) grant PB97-0220-C02.

## REFERENCES

- Alcock, C., et al., 1997, ApJ, 486, 697  
 Alcock, C., et al., 1998, ApJ, 499, L9  
 Alcock, C., et al., 2000, ApJ, 542, 281  
 Chang, K., Refsdal, S., 1984, A&A 132, 168  
 Colley, W. N., Schild, R. E., 2000, ApJ 540, 104  
 Goicoechea, L. J., Oscoz, A., Mediavilla, E., Buitrago, J., Serrà-Ricart, M., 1998, ApJ 492, 74 (G98)  
 Gould, A., 1997, Astronomical Time Series, Kluwer, Dordrecht, p. 37  
 Gould, A., Miralda-Escudé, J., 1997, ApJ, 483, L13  
 Haarsma, D. B., Hewitt, J. N., Lehár, J., Burke, B. F., 1997, ApJ 479, 102  
 Iбата, R., et al., 1999, ApJ 524, L95  
 Irwin, M. J., Webster, R. L., Hewitt, P. C., Corrigan, R. T., Jędrzejewski, R. I., 1989, AJ 98, 1989  
 Kayser, R., Refsdal, S., Stabell, R., 1986, A&A 166, 36  
 Koopmans, L. V. E., de Bruyn, A. G., 2000, in Brainerd T. G., Kochanek C. S., eds, Proc. of the Conf. "Gravitational Lensing: Recent Progress and Future Goals", in press  
 Kundić, T., Colley, W. N., Gott III, J. R., et al., 1995, ApJ 455, L5  
 Kundić, T., Turner, E. L., Colley, W. N., et al., 1997, ApJ 482, 75  
 Lasserre, T., et al., 2000, A&A 355, L39  
 Lewis, G. F., Miralda-Escudé, J., Richardson, D. C., Wambsganss, J., 1993, MNRAS 261, 647  
 Mao, S., 2000, in Brainerd T. G., Kochanek C. S., eds, Proc. of the Conf. "Gravitational Lensing: Recent Progress and Future Goals", in press  
 Oscoz, A., Serrà-Ricart, M., Goicoechea, L. J., Buitrago, J., Mediavilla, E., 1996, ApJ 470, L19

- Oscoz, A., Mediavilla, E., Goicoechea, L. J., Serra-Ricart, M.,  
Buitrago, J., 1997, ApJ 479, L89
- Paczyński, B., 1986, ApJ 301, 503
- Pelt, J., Schild, R., Refsdal, S., Stabell R., 1998, A&A 336, 829
- Pijpers, F. P., 1997, MNRAS 289, 933
- Press, W. H., Rybicki, G. B., Hewitt, J. N., 1992a, ApJ 385, 404  
(PRH92)
- Press, W. H., Rybicki, G. B., Hewitt, J. N., 1992b, ApJ 385, 416  
(PRH92)
- Press, W. H., Rybicki, G. B., 1998, ApJ 507, 108
- Rix, H. W., Franx, M., Fischer, D., Illingworth, G., 1992, AJ 104,  
959
- Schild, R. E., 1996, ApJ 464, 125 (S96)
- Schild, R. E., 1999, ApJ 514, 598
- Schild, R. E., Thomson, D. J., 1997, AJ 113, 130
- Schmidt, R., 1999, private communication
- Schmidt, R., Wambsganss, J., 1998, A&A 335, 379 (SW98)
- Schneider, P., Weiss, A., 1987, A&A 171, 49
- Serra-Ricart, M., Oscoz, A., Sanchis, T., Mediavilla, E.,  
Goicoechea, L. J., Licandro, J., Alcalde, D., Gil-Merino, R.,  
1999, ApJ 526, 40 (Paper I)
- Simonetti, J. H., Cordes, J. M., Heeschen, D. S., 1985, ApJ 296,  
46
- Sutherland, W., 1999, Rev. Mod. Phys. 71, 421
- Wambsganss, J., 1990, PhD thesis, Munich University
- Wambsganss, J., Paczyński, B., 1994, AJ 108, 1156
- Witt, H. J., 1993, ApJ 403, 530
- Wozniak, P. R., Alard, C., Udalski, A., Szmanski, M., Kubiak,  
M., Pietrzynski, G., Zebrun, K., 2000, ApJ 529, 88
- Wyithe, J. S. B., Turner, E. L., Webster, R. L., 2000, MNRAS,  
in press

This paper has been produced using the Royal Astronomical  
Society/Blackwell Science L<sup>A</sup>T<sub>E</sub>X style file.